Acta Mech 232, 135–151 (2021)
https://doi.org/10.1007/s00707-020-02811-7

ORIGINAL PAPER

B. Zhang · J. G. Yu · X. M Zhang · L. Elmaimouni

Guided wave propagating in a 1-D hexagonal piezoelectric quasi-crystal plate

Received: 15 July 2019 / Revised: 17 August 2020 / Accepted: 5 September 2020 / Published online: 20 October 2020

Abstract In the context of Bak's model, guided waves in a 1-D hexagonal piezoelectric quasi-crystal plate are investigated by applying the Legendre polynomial method. Three cases of quasi-periodic directions are discussed. The dispersion curves, phonon, and phason displacement distributions are illustrated. Some new wave phenomena are revealed: The phase velocity of Lamb wave phason modes decreases as the phonon–phason coupling parameters, R_i, increase. Phason displacements and the electric potential have consistent distributions with those of phonon displacement components in the quasi-periodic direction. These obtained results lay the theoretical basis for the design and optimization of piezoelectric devices.

1 Introduction

There existed an accepted fact that solid matters were either crystals or amorphous materials until 1980s. However, it was broken down by the discovery of a novel kind of material, i.e., quasi-crystals (QCs) with long-range orientational and quasi-periodic translational orders [1]. Due to their unique arrangement of atoms, quasi-crystals are of some desirable material properties. For example, their frictional and adhesion coefficients are quite low, but their electric resistivity, abrasion and thermal resistances are very high [2–4]. Accordingly, they have promising applications in the coating surface of engines, thin films, thermoelectric converters, electronics, communication, and so on [5,6].

As one of the important properties, the piezoelectricity of QCs has been paid increasing attention. The governing equations of piezoelectric quasi-crystal media were described by Altay et al. [7]. The piezoelasticity theory of 1-D QCs was investigated by using the operator and complex variable function methods [8]. The axial shear fracture of a transversely isotropic piezoelectric quasi-crystal cylinder was studied by Li et al. [9]. A generally loaded strip crack in a half-space of a 1-D hexagonal piezoelectric quasi-crystal was investigated by Tupholme [10]. The closed-form solutions were obtained for wedges in 1-D piezoelectric QCs by Zhang et al. [11]. Two collinear permeable anti-plane shear or mode-III cracks in a 1-D piezoelectric quasi-crystal structure were studied by Zhou and Li [12]. The mechanical and electric behaviors of 1-D piezoelectric QCs subjected to different loads were studied by Wu et al. [13].

The above references were mainly focused on static investigations. To our best knowledge, kinetic investigations are relatively rare owing to the complexity of the dynamic deformation in QCs. However, they have drawn increasing attention with increasing actual application needs. Actually, there are different opinions about the role of the phason field played in the dynamic deformation. And there exist two commonly used kinetic

B. Zhang · J. G. Yu · X. M Zhang (✉)
School of Mechanical and Power Engineering, Henan Polytechnic University, Jiaozuo 454003, People's Republic of China
E-mail: zxmworld11@hpu.edu.cn

L. Elmaimouni
LSIE-ERMAM, Faculté Polydisciplinaire d'Ouarzazate, Univ. Ibn Zohr, 45000 Ouarzazate, Marocco

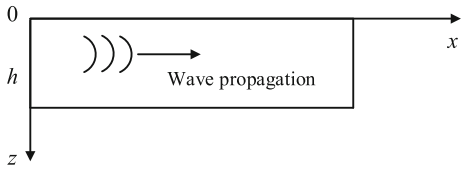

Fig. 1 Schematic diagram of an infinite 1-D hexagonal piezoelectric quasi-crystal plate

models: the Bak's and elasto-hydrodynamic models. As for the Bak's model [14], the phason field is in analogy to the phonon field that obeys Newton's second law. Owing to its simple mathematical description, it is the most one used by scholars. A moving shear crack in 1-D piezoelectric QCs was investigated by Tupholme [15]. The free vibration and harmonic response to a patch loading for layered 1-D quasi-crystal plates were investigated, respectively in [16–18]. The bending analysis in a 1-D orthorhombic quasi-crystal plate under static and transient dynamic loads was investigated by Sladekv et al. [19] utilizing the meshless Petrov–Galerkin method.

On the other hand, the elastohydrodynamic model suggests that the phason field obeys the diffusion law rather than the conservation law. The wave propagation in quasi-crystal reinforced aluminum structures was investigated by Chellappan et al. [20]. A general solution for 2-D quasi-crystal structures was obtained by Li [21]. Chiang et al. [22] proposed the local radial basis function collocation method for the plate bending analysis in orthorhombic QCs under static and transient dynamic loads.

From the above simple review, only few references about guided waves in the piezoelectric quasi-crystal structures are available so far. It is well-known that the performance of piezoelectric devices has a close relationship with wave characteristics including wave shapes, cut-off frequency, and so on. Therefore, for the purpose of design and optimization of piezoelectric devices, guided wave characteristics in a 1-D hexagonal piezoelectric quasi-crystal plate are investigated by applying the Legendre polynomial method. Owing to its simple mathematical description, Bak's model is chosen in this paper. The traction-free and open-circuit boundary conditions are assumed.

2 Mathematics and formulation

The schematic diagram of a 1-D hexagonal piezoelectric quasi-crystal plate in the Cartesian coordinate system (x, y, z) is illustrated in Fig. 1. Its thickness is h. Guided waves are propagating in the x-direction.

There exist three kinds of coupled fundamental fields in the piezoelectric QCs: the phonon, phason, and electric fields. In the context of Bak's model, the kinetic equations without body forces and free charges are written as follows :

$$T_{ij,j} = \rho \ddot{u}_i, H_{ij,j} = \rho \ddot{w}_i, D_{i,i} = 0 \tag{1}$$

where T_{ij}, H_{ij}, and D_i are phonon stresses, phason stresses, and electric displacements, respectively. u_i and w_i are the displacements in the phonon and phason fields, respectively. ρ represents the density.

The extended relationship of the strain displacement can be denoted as follows:

$$\varepsilon_{ij} = \frac{1}{2}\left(\frac{\partial u_i}{\partial x_j} + \frac{\partial u_j}{\partial x_i}\right), \quad w_{ij} = \frac{\partial w_i}{\partial x_j} \quad , \quad E_i = -\frac{\partial \phi}{\partial x_i} \tag{2}$$

where ϕ is the electric potential. ε_{ij} and w_{ij} are the phonon and phason strains, respectively. E_i represents the electric field.

As for the 1-D hexagonal piezoelectric quasi-crystal plate, if its quasi-periodic direction is identical to the z-direction, and the other two directions are periodic, it is defined as the z-direction quasi-crystal plate in this paper. By that analogy, there are the x- and y-direction quasi-crystal plates. Therefore, the wave propagation in these three cases is analyzed in detail.

2.1 The z-direction piezoelectric quasi-crystal plate

As for the z-direction quasi-crystal plate, its polarized and thickness directions are both identical with the z-direction. Only phason displacements in the $z-$direction are existing, and phason displacements in x- and y-direction vanish.

The generalized constitutive equations for the z-direction piezoelectric quasi-crystal plate are written as follows [23]:

$$\begin{aligned}
T_{xx} &= \left(C_{11}\varepsilon_{xx} + C_{12}\varepsilon_{yy} + C_{13}\varepsilon_{zz} + R_1 w_{zz} - e_{31}E_z\right)\pi(z),\\
T_{yy} &= \left(C_{12}\varepsilon_{xx} + C_{22}\varepsilon_{yy} + C_{13}\varepsilon_{zz} + R_1 w_{zz} - e_{31}E_z\right)\pi(z),\\
T_{zz} &= \left(C_{13}\varepsilon_{xx} + C_{13}\varepsilon_{yy} + C_{33}\varepsilon_{zz} + R_2 w_{zz} - e_{33}E_z\right)\pi(z),\\
T_{yz} &= \left(2C_{44}\varepsilon_{yz} + R_3 w_{zy} - e_{15}E_y\right)\pi(z),\\
T_{xz} &= \left(2C_{55}\varepsilon_{xz} + R_3 w_{zx} - e_{15}E_x\right)\pi(z),\\
T_{xy} &= 2C_{66}\varepsilon_{xy}\pi(z),
\end{aligned} \tag{3.1}$$

$$\begin{aligned}
H_{zz} &= \left(R_1\varepsilon_{xx} + R_1\varepsilon_{yy} + R_2\varepsilon_{zz} + K_1 w_{zz} - d_{33}E_z\right)\pi(z),\\
H_{zx} &= \left(2R_3\varepsilon_{xz} + K_2 w_{zx} - d_{15}E_x\right)\pi(z),\\
H_{zy} &= \left(2R_3\varepsilon_{yz} + K_2 w_{zy} - d_{15}E_y\right)\pi(z),
\end{aligned} \tag{3.2}$$

$$\begin{aligned}
D_z &= \left[e_{31}\left(\varepsilon_{xx} + \varepsilon_{yy}\right) + e_{33}\varepsilon_{zz} + d_{33}w_{zz} + \in_{33} E_z\right]\pi(z),\\
D_x &= \left[2e_{15}\varepsilon_{zx} + d_{15}w_{zx} + \in_{11} E_x\right]\pi(z),\\
D_y &= \left[2e_{15}\varepsilon_{zy} + d_{15}w_{zy} + \in_{11} E_y\right]\pi(z)
\end{aligned} \tag{3.3}$$

where $\pi(z)$ is a window function to be described later. C_{ij} and e_{ij} are elastic and piezoelectric coefficients in the phonon field, respectively. K_i and d_{ij} represent elastic and piezoelectric coefficients in the phason field, respectively. R_i represent the phonon–phason coupling coefficients, and $\in_{ij}$ represent dielectric coefficients.

For the assumed traction-free and open-circuit boundary condition, it is required that displacements and electric potential at the upper and bottom surfaces do not vanish, normal stress components and electric displacement vanish,

$$T_{xz} = T_{yz} = T_{zz} = H_{zz} = D_z = 0 \quad \text{at } z = 0 \text{ and } z = h. \tag{4}$$

To deal with it, a rectangle window function $\pi(z)$ is introduced in Eq. (3.1), which can be written as:

$$\pi(z) = \begin{cases} 1, & 0 \le z \le h \\ 0, & \text{elsewhere} \end{cases}. \tag{5}$$

Actually, it is the subtraction of two Heaviside functions. Its derivative is $\delta(z) - \delta(z-h)$ with $\delta(z)$ being an impulse function, i.e., $\delta(z) - \delta(z-h) = 0$. Therefore, material parameters become position-dependent physical constants. When substituted in the field equations, they lead by derivatives to delta functions multiplying the normal stress components, thus ensuring that the normal stresses vanish at the boundaries, and other stresses may vanish or not.

Thus, the assumed boundary conditions are automatically incorporated into the constitutive equations. The explanation of this method to deal with boundary conditions are detailed in Ref. [24].

For harmonic waves propagating in the x-direction, phonon and phason displacements, electric potential can be denoted as follows:

$$\begin{aligned}
&u_x = U(z)e^{ikx-i\omega t}, \quad u_y = V(z)e^{ikx-i\omega t}, \quad u_z = W(z)e^{ikx-i\omega t},\\
&w_z = \gamma(z)e^{ikx-i\omega t}, \quad \phi = X(z)e^{ikx-i\omega t}
\end{aligned} \tag{6}$$

where $U(z)$, $V(z)$, $W(z)$, and $\gamma(z)$ represent the phonon and phason displacement amplitudes, respectively. $X(z)$ is the amplitude of the electric potential.

Subsequently, substituting Eqs. (2–6) into Eq. (1), the following differential equations can be obtained:

$$\begin{aligned}
&\pi(z)[-C_{11}k^2U + C_{55}U'' + (C_{13}+C_{55})ikW' + (R_1+R_3)ik\gamma' + (e_{15}+e_{31})ikX']\\
&\quad +[\delta(z-0) - \delta(z-h)][C_{55}U' + C_{55}ikW + R_3ik\gamma + e_{15}ikX] = -\rho\omega^2 U,
\end{aligned} \tag{7.1}$$

$$\pi(z)[-C_{66}k^2V + C_{44}V''] + C_{44}V'[\delta(z-0) - \delta(z-h)] = -\rho\omega^2 V, \tag{7.2}$$

$$\pi(z)[(C_{13}+C_{55})ikU' - C_{55}k^2W + C_{33}W'' - R_3k^2\gamma + R_2\gamma'' - e_{15}k^2X + e_{33}X'']$$
$$+[\delta(z-0)-\delta(z-h)][C_{13}ikU + C_{33}W' + R_2\gamma' + e_{33}X'] = -\rho\omega^2 W, \tag{7.3}$$
$$\pi(z)[(R_1+R_3)ikU' - R_3k^2W + R_2W'' - K_2k^2\gamma + K_1\gamma'' - d_{15}k^2X + d_{33}X'']$$
$$+[\delta(z-0)-\delta(z-h)][R_1ikU + R_2W' + K_1\gamma' + d_{33}X'] = -\rho\omega^2\gamma, \tag{7.4}$$
$$\pi(z)[(e_{15}+e_{31})ikU' - e_{15}k^2W + e_{33}W'' - d_{15}k^2\gamma + d_{33}\gamma'' + \in_{11} k^2X - \in_{33} X'']$$
$$+[\delta(z-0)-\delta(z-h)][e_{31}ikU + e_{33}W' + d_{33}\gamma' - \in_{33} X'] = 0 \tag{7.5}$$

where the dash denotes the derivative with respect to the depth z. Obviously, Eq. (7.2) is independent of electric and phason fields, which governs the SH waves. SH wave characteristics in this case are similar to those for crystal plates. Therefore, they are not investigated in this paper.

To solve the coupled Eq. (7.1), $U(z)$, $W(z)$, $\gamma(z)$, and $X(z)$ are expanded into the Legendre polynomial series:

$$U(z) = \sum_{m=0}^{\infty} p_m^1 Q_m(z),\ W(z) = \sum_{m=0}^{\infty} p_m^2 Q_m(z),$$
$$\gamma(z) = \sum_{m=0}^{\infty} r_m^1 Q_m(z),\ X(z) = \sum_{m=0}^{\infty} r_m^2 Q_m(z) \tag{8}$$

where p_m^i $(i=1,2)$ and r_m^i are the undetermined coefficients. $Q_m(z) = \sqrt{\frac{2m+1}{h}} P_m(\frac{2z-h}{h})$ with P_m being the mth Legendre polynomial. Theoretically, m runs from 0 to ∞. However, as a matter of fact, the above summations are truncated at some finite values $m = M$.

Multiply Eq. (7.1) by $Q_j(z)$ with j running from 0 to M. Subsequently, integrating over z from 0 to h, the following system is obtained by utilizing the orthonormality of the Legendre polynomial:

$$A_{11}^{m,j} p_m^1 + A_{12}^{m,j} p_m^2 + A_{13}^{m,j} r_m^1 + A_{14}^{m,j} r_m^2 = \omega^2 M_{m,j} p_m^1, \tag{9.1}$$
$$A_{21}^{m,j} p_m^1 + A_{22}^{m,j} p_m^2 + A_{23}^{m,j} r_m^1 + A_{24}^{m,j} r_m^2 = \omega^2 M_{m,j} p_m^2, \tag{9.2}$$
$$A_{31}^{m,j} p_m^1 + A_{32}^{m,j} p_m^2 + A_{33}^{m,j} r_m^1 + A_{34}^{m,j} r_m^2 = \omega^2 M_{m,j} r_m^1, \tag{9.3}$$
$$A_{41}^{m,j} p_m^1 + A_{42}^{m,j} p_m^2 + A_{43}^{m,j} r_m^1 + A_{44}^{m,j} r_m^2 = 0 \tag{9.4}$$

where $M_{m,j}$ and $A_{\alpha\gamma}^{m,j}$ $(\alpha, \gamma = 1,2,3)$ can be calculated from Eq. (7.1), which are detailed in the Appendix.

The following equation can be obtained from Eq. (9.4),

$$r_m^2 = -\left[A_{44}^{m,j}\right]^{-1} (A_{41}^{m,j} p_m^1 + A_{42}^{m,j} p_m^2 + A_{43}^{m,j} r_m^1). \tag{10}$$

Subsequently, Eq. (9.1) can be transformed into the following matrix system by substituting Eq. (10) into Eq. (9.1):

$$\begin{bmatrix} \bar{A}_{11}^{m,j} & \bar{A}_{12}^{m,j} & \bar{A}_{13}^{m,j} \\ \bar{A}_{21}^{m,j} & \bar{A}_{22}^{m,j} & \bar{A}_{22}^{m,j} \\ \bar{A}_{31}^{m,j} & \bar{A}_{32}^{m,j} & \bar{A}_{33}^{m,j} \end{bmatrix} \begin{Bmatrix} p_m^1 \\ p_m^2 \\ r_m^1 \end{Bmatrix} = \omega^2 \begin{bmatrix} M_{m,j} & 0 & 0 \\ 0 & M_{m,j} & 0 \\ 0 & 0 & M_{m,j} \end{bmatrix} \begin{Bmatrix} p_m^1 \\ p_m^2 \\ r_m^1 \end{Bmatrix}. \tag{11}$$

Up to now, the problem is transformed as an eigenvalue problem to be solved. The values of ω are square roots of the eigenvalues. The profiles of the phonon and phason displacement components can be obtained according to the eigenvectors. They are calculated by standard computer programs written in the software "Mathematica" .

In Eq. (11), k is a known quantity. Therefore, corresponding eigenvalues can be obtained and written as $\omega[k]$ for a known k. Thus, the phase velocity is calculated by

$$V_{ph} = \frac{\omega[k]}{k}. \tag{12}$$

Similarly, the eigenvectors $\left\{ p_m^1 \;\; p_m^2 \;\; r_m^1 \right\}^T$ can be obtained for a known k. Then, substituting them into Eq. (10), r_m^2 can be obtained. Subsequently, substituting $\left\{ p_m^1 \;\; p_m^2 \;\; r_m^1 \;\; r_m^2 \right\}^T$ into Eq. (8), phonon and phason displacement components and the electric potential can be obtained.

2.2 The x-direction piezoelectric quasi-crystal plate

In this case, only phason displacements in the x-direction are existing, phason displacements in the z- and y-directions vanish, i.e., $w_z = w_y = 0$.

The generalized constitutive equations of the x-direction piezoelectric quasi-crystal plate can be denoted as follows:

$$\begin{aligned}
T_{yy} &= \left(C_{11}\varepsilon_{yy} + C_{12}\varepsilon_{zz} + C_{13}\varepsilon_{xx} + R_1 w_{xx} - e_{31}E_x\right)\pi\,(z)\,,\\
T_{zz} &= \left(C_{12}\varepsilon_{yy} + C_{22}\varepsilon_{zz} + C_{13}\varepsilon_{xx} + R_1 w_{xx} - e_{31}E_x\right)\pi\,(z)\,,\\
T_{xx} &= \left(C_{13}\varepsilon_{yy} + C_{13}\varepsilon_{zz} + C_{33}\varepsilon_{xx} + R_2 w_{xx} - e_{33}E_x\right)\pi\,(z)\,,\\
T_{yz} &= 2C_{66}\varepsilon_{yz}\pi\,(z)\,,\\
T_{xz} &= (2C_{44}\varepsilon_{xz} + R_3 w_{xz} - e_{15}E_z)\,\pi\,(z)\,,\\
T_{xy} &= (2C_{44}\varepsilon_{xy} + R_3 w_{xy} - e_{15}E_y)\pi\,(z)\,,
\end{aligned} \tag{13.1}$$

$$\begin{aligned}
H_{xx} &= \left(R_2\varepsilon_{xx} + R_1\varepsilon_{yy} + R_1\varepsilon_{zz} + K_1 w_{xx} - d_{33}E_x\right)\pi\,(z)\,,\\
H_{xz} &= (2R_3\varepsilon_{xz} + K_2 w_{xz} - d_{15}E_z)\,\pi\,(z)\,,\\
H_{xy} &= \left(2R_3\varepsilon_{xy} + K_2 w_{xy} - d_{15}E_y\right)\pi\,(z)\,,
\end{aligned} \tag{13.2}$$

$$\begin{aligned}
D_x &= \left[e_{31}\left(\varepsilon_{zz} + \varepsilon_{yy}\right) + e_{33}\varepsilon_{xx} + d_{33}w_{xx} + \in_{33} E_x\right]\pi\,(z)\,,\\
D_z &= \left[2e_{15}\varepsilon_{xz} + d_{15}w_{xz} + \in_{11} E_z\right]\pi\,(z)\,,\\
D_y &= \left[2e_{15}\varepsilon_{xy} + d_{15}w_{xy} + \in_{11} E_y\right]\pi\,(z)\,.
\end{aligned} \tag{13.3}$$

Its phonon displacements and electric potential are the same as those for the z-direction quasi-crystal plate, and the phason displacement can be denoted as:

$$w_x = \alpha(z)e^{ikx - i\omega t} \tag{14}$$

where $\alpha(z)$ is the phason displacement amplitude in the x-direction.

Substituting Eqs. (2) and (13.1–14) into Eq. (1), differential equations can be obtained:

$$\begin{aligned}
&\pi(z)[-C_{33}k^2U + C_{44}U'' + (C_{13} + C_{44})ikW' - R_2k^2\alpha + R_3\alpha'' - e_{33}k^2X + e_{15}X'']\\
&\quad + [\delta(z-0) - \delta(z-h)][C_{44}U' + C_{44}ikW + R_3\alpha' + e_{15}X'] = -\rho\omega^2 U, \qquad (15.1)\\
&\pi(z)[-C_{44}k^2V + C_{66}V''] + C_{66}V'[\delta(z-0) - \delta(z-h)] = -\rho\omega^2 V, \qquad (15.2)\\
&\pi(z)[(C_{13} + C_{44})ikU' - C_{44}k^2W + C_{22}W'' + (R_3 + R_1)ik\alpha' + (e_{15} + e_{31})ikX']\\
&\quad + [\delta(z-0) - \delta(z-h)][C_{13}ikU + C_{22}W' + R_1ik\alpha + e_{31}X'] = -\rho\omega^2 W, \qquad (15.3)\\
&\pi(z)[(R_1 + R_3)ikW' - R_2k^2U + R_3U'' - K_1k^2\alpha + K_2\alpha'' - d_{33}k^2X + d_{15}X'']\\
&\quad + [\delta(z-0) - \delta(z-h)][R_3ikW + R_3U' + K_2\alpha' + d_{15}X'] = -\rho\omega^2\alpha, \qquad (15.4)\\
&\pi(z)[(e_{15} + e_{31})ikW' - e_{33}k^2U + e_{15}U'' - d_{33}k^2\alpha + d_{15}\alpha'' + \in_{33} k^2X - \in_{11} X'']\\
&\quad + [\delta(z-0) - \delta(z-h)][e_{15}U' + e_{15}ikW + d_{15}\alpha' - \in_{11} X'] = 0. \qquad (15.5)
\end{aligned}$$

Specifically, SH waves are also independent of the phason and electric fields in this case. The following detailed solving procedure is similar to that in Sect. 2.1. Therefore, it is not shown to save space.

2.3 The y-direction piezoelectric quasi-crystal plate

In this case, only phason displacements in the y-direction are existing, phason displacements in the x- and z-directions vanish, i.e., $w_z = w_x = 0$.

Its phonon displacements and electric potential are the same as those for z-direction quasi-crystal plates, and phason displacements can be denoted as:

$$w_y = \beta(z)e^{ikx-i\omega t} \tag{16}$$

where $\beta(z)$ is the phason displacement amplitude in the y-direction.

The generalized constitutive equations are as follows:

$$\begin{aligned}
T_{zz} &= \left[C_{11}\varepsilon_{zz} + C_{12}\varepsilon_{xx} + C_{13}\varepsilon_{yy} + R_1 w_{yy} - e_{31}E_y\right]\pi(z),\\
T_{xx} &= \left[C_{12}\varepsilon_{zz} + C_{22}\varepsilon_{xx} + C_{13}\varepsilon_{yy} + R_1 w_{yy} - e_{31}E_y\right]\pi(z),\\
T_{yy} &= \left[C_{13}\varepsilon_{zz} + C_{13}\varepsilon_{xx} + C_{33}\varepsilon_{yy} + R_2 w_{yy} - e_{33}E_y\right]\pi(z),\\
T_{xz} &= 2C_{66}\varepsilon_{xz}\pi(z),\\
T_{xy} &= \left[2C_{44}\varepsilon_{xy} + R_3 w_{yx} - e_{15}E_x\right]\pi(z),\\
T_{yz} &= \left[2C_{44}\varepsilon_{yz} + R_3 w_{yz} - e_{15}E_z\right]\pi(z),
\end{aligned} \tag{17.1}$$

$$\begin{aligned}
H_{yy} &= \left[R_2\varepsilon_{yy} + R_1\varepsilon_{zz} + R_1\varepsilon_{xx} + K_1 w_{yy} - d_{33}E_y\right]\pi(z),\\
H_{yx} &= \left[2R_3\varepsilon_{yx} + K_2 w_{yx} - d_{15}E_x\right]\pi(z),\\
H_{yz} &= \left[2R_3\varepsilon_{yz} + K_2 w_{yz} - d_{15}E_z\right]\pi(z),
\end{aligned} \tag{17.2}$$

$$\begin{aligned}
D_y &= \left[e_{31}(\varepsilon_{zz} + \varepsilon_{xx}) + e_{33}\varepsilon_{yy} + d_{33}w_{yy} + \in_{33} E_y\right]\pi(z),\\
D_x &= \left[2e_{15}\varepsilon_{yx} + d_{15}w_{yx} + \in_{11} E_x\right]\pi(z),
\end{aligned} \tag{17.3}$$

Subsequently, substituting Eqs. (2) and (16–17.1) into Eq. (1), the following equations are obtained:

$$\begin{aligned}
&\pi(z)[-C_{22}k^2U + C_{66}U'' + (C_{12} + C_{66})ikW'] \\
&\quad + [\delta(z-0) - \delta(z-h)][C_{66}U' + C_{66}ikW] = -\rho\omega^2 U,
\end{aligned} \tag{18.1}$$

$$\begin{aligned}
&\pi(z)(-C_{44}k^2V + C_{44}V'' - R_3k^2\beta + R_3\beta'' - e_{15}k^2X + e_{15}X'') \\
&\quad + (C_{44}V' + R_3\beta' + e_{15}X')[\delta(z-0) - \delta(z-h)] = -\rho\omega^2 V,
\end{aligned} \tag{18.2}$$

$$\begin{aligned}
&\pi(z)[(C_{12} + C_{66})ikU' - C_{66}k^2W + C_{11}W''] \\
&\quad + [\delta(z-0) - \delta(z-h)][C_{12}ikU + C_{11}W'] = -\rho\omega^2 W,
\end{aligned} \tag{18.3}$$

$$\begin{aligned}
&\pi(z)(-R_3k^2V + R_3V'' - K_2k^2\beta + K_2\beta'' - d_{15}k^2X - d_{15}X'') \\
&\quad + (R_3V' + K_2\beta' - d_{15}X')[\delta(z-0) - \delta(z-h)] = -\rho\omega^2\beta,
\end{aligned} \tag{18.4}$$

$$\begin{aligned}
&\pi(z)(-e_{15}k^2V + e_{15}V'' - d_{15}k^2\beta + d_{15}\beta'' + \in_{11} k^2X - \in_{11} X'') \\
&\quad + (e_{15}V' + d_{15}\beta' - \in_{11} X')[\delta(z-0) - \delta(z-h)] = 0.
\end{aligned} \tag{18.5}$$

It can be observed that Eqs. (18.1) and (18.3) are coupled and independent of the phonon and electric fields. Actually, they govern Lamb waves having the same wave characteristics with elastic Lamb waves in the crystal plates. SH waves are governed by the other equations that are coupled with the phason and electric fields.

The detailed solving procedure is similar to that in the Sect. 2.1. Therefore, it is not shown to save space.

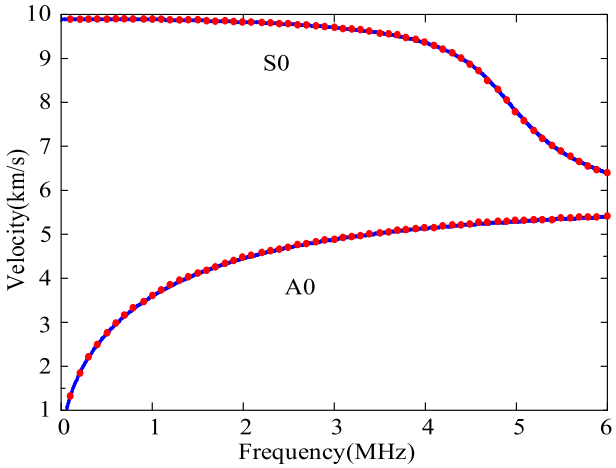

Fig. 2 Phase velocity dispersion curves for the piezoelectric crystal plate. The lines: the Legendre polynomial method; the dotted lines: the Peano-series method

3 Numerical results

As above mentioned, SH waves in the x- and z-direction quasi-crystal plates, and Lamb waves in the y-direction quasi-crystal plates are independent of the phason and electric fields. Therefore, to investigate the phonon–phason coupling and piezoelectric effects on wave characteristics, Lamb waves in the x- and z-direction quasi-crystal plates, and SH waves in the y-direction quasi-crystal plates are investigated in this paper, respectively.

3.1 Confirmation of the present method

To our best knowledge, investigations about the guided wave propagation in the piezoelectric quasi-crystal plates are rare. However, if the phason field is absent, the piezoelectric quasi-crystal plate can be reduced to the piezoelectric crystal plate. Therefore, to confirm the correctness of the present method in a special case, the phason field is assumed to be absent, i.e., $R_i = K_{ij} = d_{ij} = 0$, to make a comparison with results obtained from the Peano-series method [25]. The corresponding material parameters are the same as those in Ref. [25]. The dispersion curves are illustrated in Fig. 2. The lines are results obtained from the present method, the dotted lines are results obtained from the Peano-series method. Figure 2 shows that results obtained from these two methods are in perfect agreement.

3.2 Lamb waves in the z-direction piezoelectric quasi-crystal plates

3.2.1 The influence of the phason field on wave characteristics

In this Subsection, Lamb waves propagating in the z-direction piezoelectric quasi-crystal plates are firstly investigated. Their material parameters are listed in Table 1 [13]. For brevity, the undermentioned structures are all z-direction piezoelectric quasi-crystal plates unless otherwise specified.

Firstly, the phonon–phason coupling effect is taken into account. Figure 3 shows its phason velocity dispersion curves. Lines are results for the piezoelectric quasi-crystal plate, and dotted lines are results for the piezoelectric crystal plate, i.e., $R_i = K_{ij} = d_{ij} = 0$ with other parameters being unaltered. It is worth noting that the phonon–phason coupling effect on the dispersion curves is significant: Firstly, there are always some modes in Fig. 3 corresponding to elastic wave modes in the piezoelectric crystal plate, which are attributed to the phonon field. It is well-known that the phonon field is responsible for the macroscopic deformation of quasi-crystal materials, which plays the same role as the elastic field in crystal materials. Therefore, these modes are described as phonon modes. Meanwhile, like Lamb waves in crystal plates, they can also be divided into symmetrical and anti-symmetrical modes, which can be distinguished according to displacement distributions in Fig. 5. Therefore, they are named as A0 mode, S0 mode….. There is a class of independent modes that are

Table 1 Material parameters of the z-direction piezoelectric quasi-crystal material

Property	C_{11}	C_{12}	C_{13}	C_{22}	C_{23}	C_{33}	C_{44}	C_{55}
	23.433	5.741	6.663	23.433	6.663	23.222	7.019	7.019
	C_{66}	ρ	R_1	R_2	R_3	K_1	K_2	e_{15}
	8.846	4.186	0.8846	0.8846	0.8846	12.2	2.4	11.6
	e_{31}	e_{33}	e_{24}	d_{15}	d_{33}	d_{24}	$\in_{11}$	$\in_{33}$
	-4.4	18.6	11.6	1.16	1.86	1.16	5	10

Units: $C_{ij}\,(10^{10}\,\mathrm{N/m^2})$, $\rho\,(10^3\,\mathrm{kg/m^3})$, $R_i\,(10^9\,\mathrm{N/m^2})$, $K_i\,(10^{10}\,\mathrm{N/m^2})$, $e_{ij}\,(\mathrm{C/m^2})$, $d_{ij}\,(\mathrm{c/m^2})$, $\in_{ij}\,(10^{-9}\,\mathrm{C^2/(N\,m^2)})$

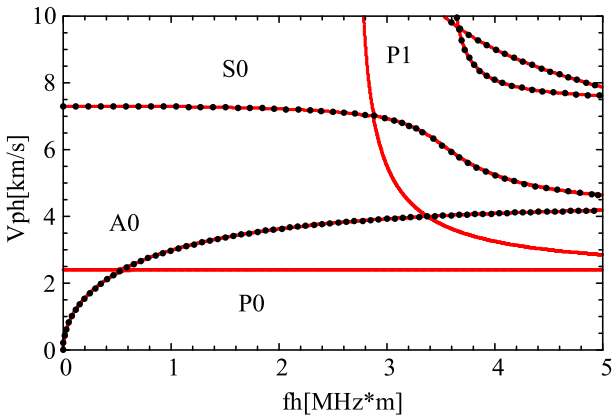

Fig. 3 Phase velocity dispersion curves lines: the piezoelectric quasi-crystal plate; dotted lines: the piezoelectric crystal plate

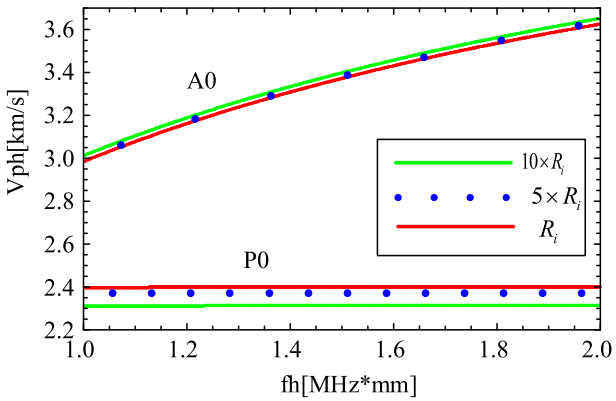

Fig. 4 Phonon–phason coupling effect on dispersion curves

attributed to the phason field. Here, they are described as phason modes, i.e., P0 mode, P1 mode….. Moreover, in comparison with Fig. 2, the first three modes have no cutoff frequencies for the piezoelectric quasi-crystal plate, not as to the first two modes without cutoff frequencies for the piezoelectric crystal plate. Furthermore, the lines and dotted lines are almost overlapped, i.e., the phonon–phason coupling effect on phonon modes is extremely weak. The reason lies in the fact that phonon–phason coupling parameters R_i in Table 1 are much smaller than elastic coefficients C_{ij} in the phonon field.

Then, the phonon–phason coupling coefficients are all multiplied by 5 and 10, respectively. Their phase velocity dispersion curves of the first two modes are illustrated in Fig. 4. The influences on other modes are similar. Therefore, no Figures are shown here. For the phonon modes, the phonon–phason coupling effect increases, and phase velocity increases at high frequencies as the phonon–phason coupling coefficients R_i increase. Besides, the phonon–phason coupling effect on phason modes is more significant than that of phonon modes, and phase velocity decreases as the phonon–phason coupling coefficients R_i increase.

Subsequently, the phonon and phason displacement, electric potential distributions of the first three modes at $kh = 0.5$ are illustrated in Fig. 5. It can be seen that, for the phonon modes, amplitudes of phonon displacements are far larger than those of phason displacements, i.e., energies are mainly concentrated in phonon displacement

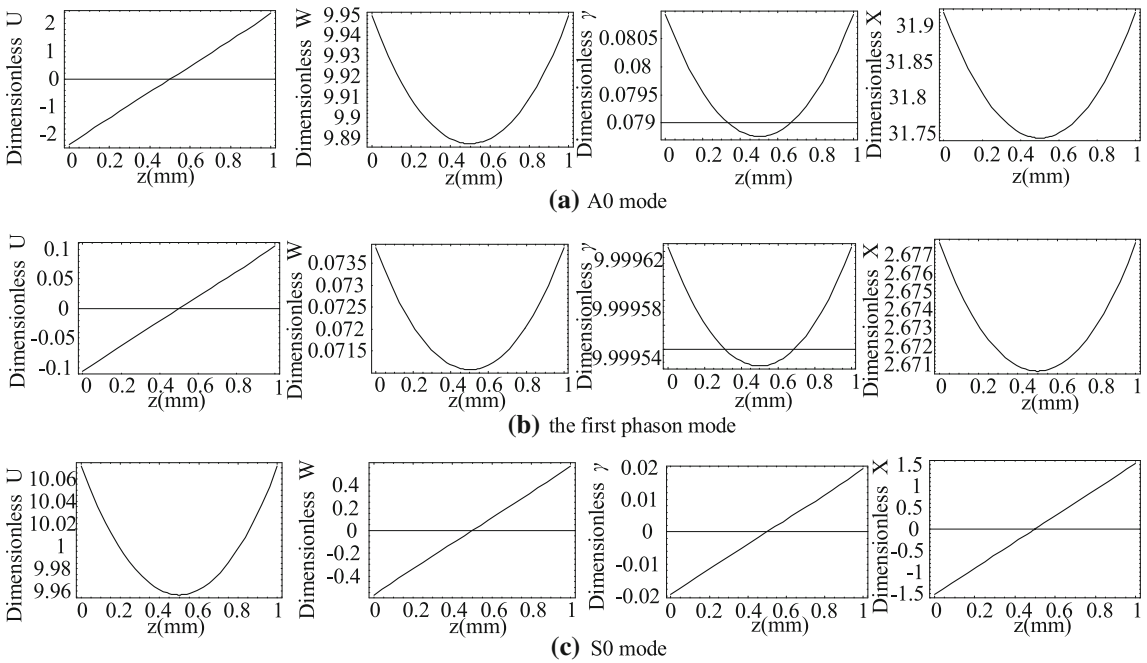

Fig. 5 Displacement and electric potential distributions of the first three modes at $kh = 0.5$

components. However, for the phason modes, amplitudes of phason displacements are far larger than those of phonon displacements, i.e., energies are mainly concentrated in phason displacement components. This phenomenon is also attributed to the weak phonon–phason coupling. Furthermore, phason displacements and electric potential distributions have the same symmetry with those of the phonon displacement components W in the quasi-periodic direction. It lies in the fact that some terms in Eq. (7.1) related to phason displacements and electric potential are similar to those of phonon displacement components in the z-direction.

3.2.2 The piezoelectric effect on wave characteristics

As above mentioned, there are coupled phonon, phason, and electric fields in the 1-D hexagonal piezoelectric quasi-crystal plate. Therefore, in addition to the phonon–phason coupling effect, it also exhibits the electro-phonon and electro-phason coupling effects. In this Subsection, it is necessary to investigate piezoelectric effects on wave characteristics in the phonon and phason fields, respectively. Firstly, the phase velocity dispersion curves of the piezoelectric and elastic quasi-crystal plates are illustrated in Fig. 6. Like the piezoelectric crystal case [26], the phase velocity of phonon and phason modes in the piezoelectric quasi-crystal plate is higher than that of the elastic quasi-crystal plate owing to the piezoelectric effects. Furthermore, the piezoelectric effect in the phonon field is more considerable than that in the phason field. It lies in the reason that piezoelectric parameters e_{ij} in the phonon field in Table 1 are larger than piezoelectric parameters d_{ij} in the phason field.

It is well known that the piezoelectric effect has a close relationship with material parameters in the electric field. Therefore, due to the phonon–phason coupling effect, the influence of material parameters in the electric field on piezoelectric effects is studied. Firstly, the influence of piezoelectric parameters in the phonon field is investigated. The piezoelectric parameters e_{ij} in the phonon field are multiplied by 3 and 5, respectively. Other parameters remain unchanged. Figure 7 shows that the influence of e_{ij} on two piezoelectric effects is opposite. For the phonon modes, the phase velocity increases with the increase of e_{ij}. The piezoelectric effect in the phonon field has a positive correlation with e_{ij}, which is consistent with the case of the piezoelectric crystal plate. For the phason modes, phase velocity decreases with the increase of e_{ij}. The piezoelectric effect in the phason field has a negative correlation with e_{ij}. Furthermore, the influence of e_{ij} on the piezoelectric effect in the phonon field is stronger than that in the phason field, which is attributed to the difference between piezoelectric parameters in the phonon and phason fields.

Secondly, the piezoelectric parameters d_{ij} in the phason field are multiplied by 3 and 5, respectively. Other parameters remain unchanged. Figure 8 shows the corresponding dispersion curves. For the phonon modes,

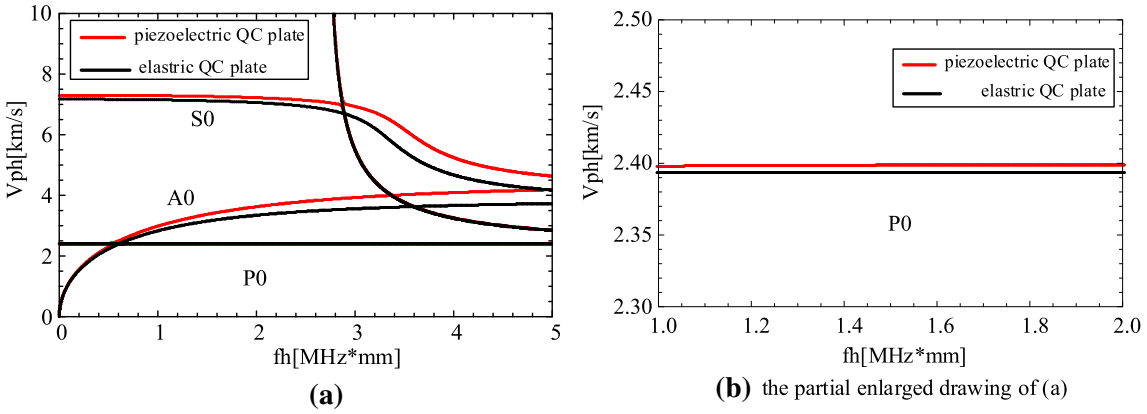

Fig. 6 Phase velocity dispersion curves for the piezoelectric and elastic quasi-crystal plates

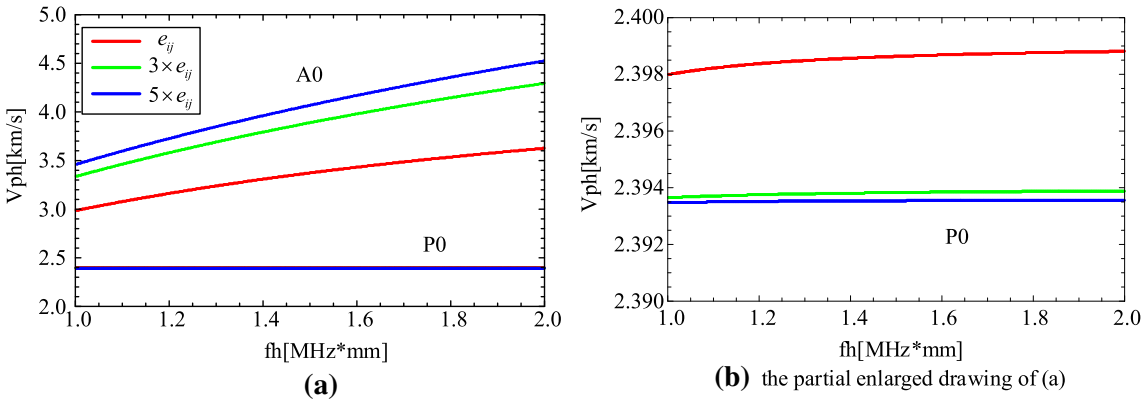

Fig. 7 Phase velocity dispersion curves for the piezoelectric quasi-crystal plate with enlarged piezoelectric parameters e_{ij} in the phonon field

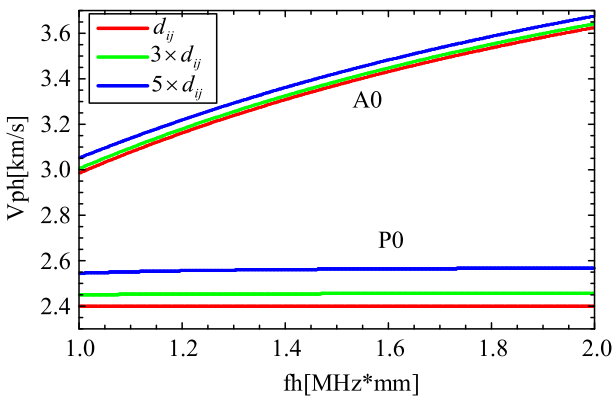

Fig. 8 Phase velocity dispersion curves for the piezoelectric quasi-crystal plate with enlarged piezoelectric parameters d_{ij} in the phason field

the phase velocity increases at high frequencies with the increase of d_{ij}. For the phason modes, the phase velocity always increases with the increase of d_{ij}. Furthermore, the influence of piezoelectric parameters d_{ij} on the phonon modes is weaker than that on the phason modes. Besides, compared with Fig. 7, the influences of the piezoelectric parameters e_{ij} and d_{ij} on the phason modes are opposite.

At last, dielectric coefficients $\in_{ij}$ are multiplied by 3 and 5, respectively. Other parameters remain unchanged. Figure 9 shows the corresponding dispersion curves. For all phonon and phason modes, the phase velocity always decreases as the dielectric coefficients $\in_{ij}$ increase, i.e., the piezoelectric effects are negatively related to the dielectric coefficients, which is consistent with this for the piezoelectric crystal plate.

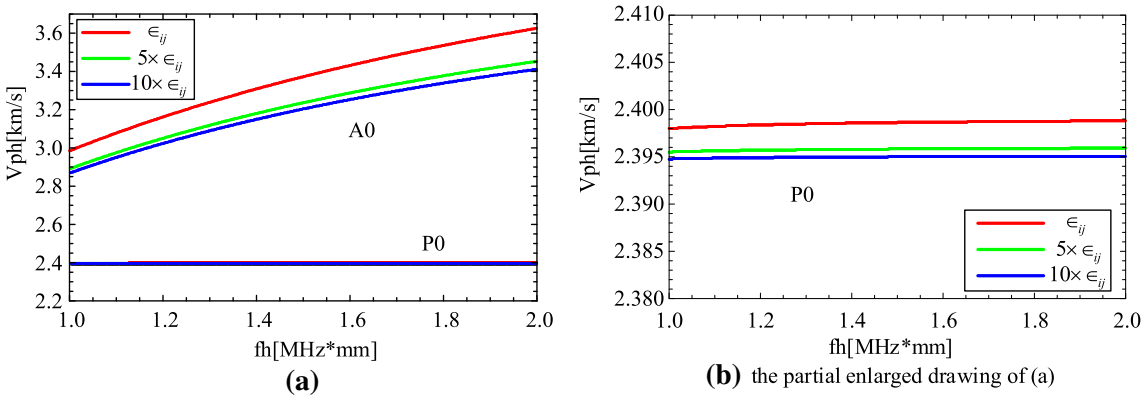

Fig. 9 Phase velocity dispersion curves for the piezoelectric quasi-crystal plate with enlarged dielectric coefficients $\in_{ij}$ in the phason field

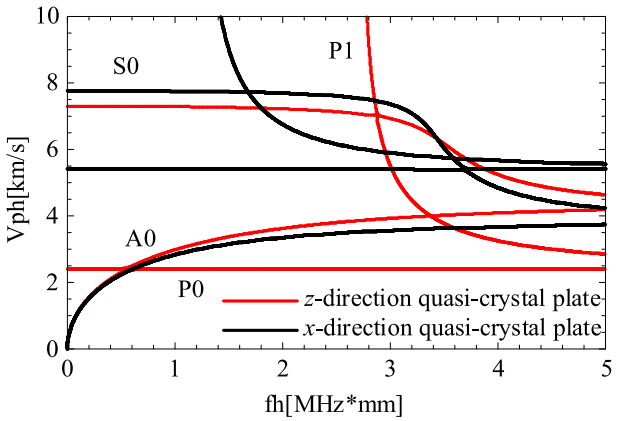

Fig. 10 Phase velocity dispersion curves for x- and z-direction piezoelectric quasi-crystal plates

3.3 Lamb waves propagating in the x-direction piezoelectric quasi-crystal plate

In this Subsection, Lamb waves propagating in the x-direction piezoelectric quasi-crystal plates are investigated. In this case, the quasi-periodic and polarization directions are all changed. Figure 10 shows the corresponding dispersion curves. It can be seen that the quasi-periodic and polarization directions have significant influence on the dispersion curves. Furthermore, their influences on different modes are different. For the phonon modes, their influences are complex. For example, the phase velocity of the S0 mode increases at low frequencies, and decreases at high frequencies. For the phason modes, the phase velocity of the x-direction piezoelectric quasi-crystal plate is far larger than that of the z-direction piezoelectric quasi-crystal plate.

Figure 11 shows the phonon and phason displacement, electric potential distributions of the first three modes at $kh = 0.5$ for the x-direction piezoelectric quasi-crystal plate. Compared with Fig. 5, the differences of the phason displacement distributions are significant. It can be observed that the phason displacement and electric potential distributions have the same symmetry with those of the phonon displacement components U in the quasi-periodic direction. The reason lies in the fact that some terms in Eq. (15.1) related to the phason displacement and electric potential are similar to those of the phonon displacement components U in the x-direction. Furthermore, for the phonon modes, the amplitudes of the phason displacements are smaller than those of the phonon displacements. It is opposite to the phason modes.

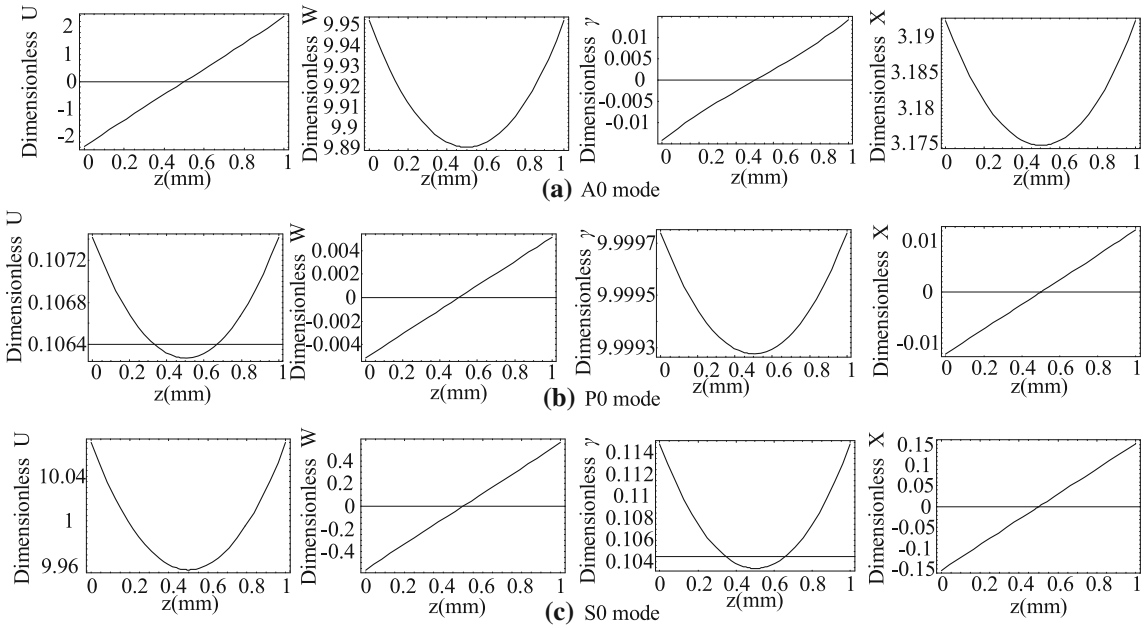

Fig. 11 Displacement and electric potential distributions of the first three modes at $kh = 0.5$ for x-direction piezoelectric quasi-crystal plates

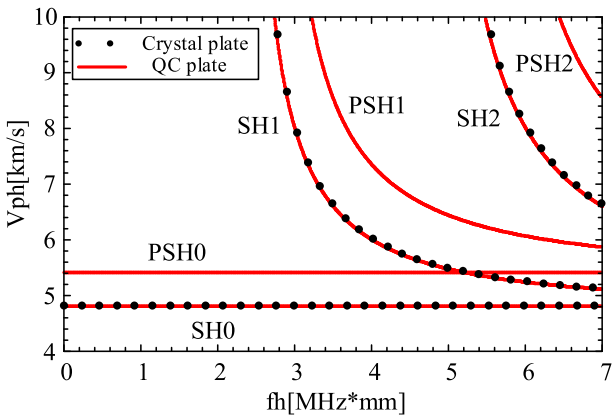

Fig. 12 Phase velocity dispersion curves of SH waves

3.4 SH waves propagating in the y-direction piezoelectric quasi-crystal plate

3.4.1 The influence of the phason field

Firstly, the phonon–phason coupling effect on SH waves is investigated. Figure 12 shows dispersion curves of the piezoelectric quasi-crystal and crystal plates ($R_i = K_i = 0$ and other material parameters are unchanged). There are some modes in Fig. 12 corresponding to elastic wave modes in the piezoelectric crystal plate, which is mainly governed by the phonon field. Therefore, these modes are described as SH phonon modes, i.e., SH0 mode, SH1 mode…. There is a class of independent modes attributed to the phason field. Here, they are described as SH phason modes, i.e., PSH0 mode, PSH1 mode …. Moreover, the phonon–phason coupling effect on SH phonon modes is also extremely weak. Furthermore, trends of phonon and phason modes are consistent, i.e., they have similar wave characteristics, such as displacement distributions, which is shown in Fig. 14 in detail.

Subsequently, the influence of phonon–phason coupling coefficients R_i on dispersion curves of SH waves is illustrated in Fig. 13. Their influences on phonon and phason modes are opposite, i.e., as R_i increase, the phase velocity of the phonon modes decreases, and the phase velocity of the phason modes increases.

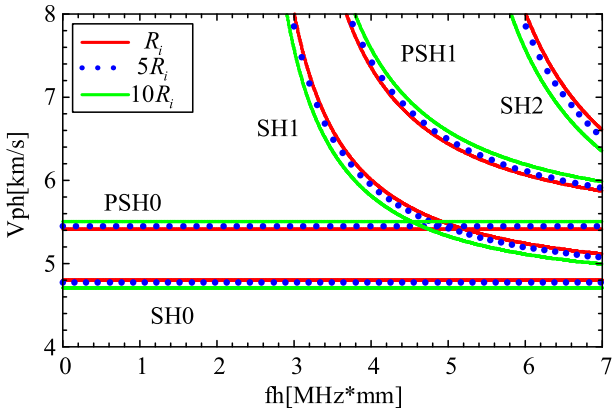

Fig. 13 The phonon–phason coupling effect on dispersion curves of SH waves

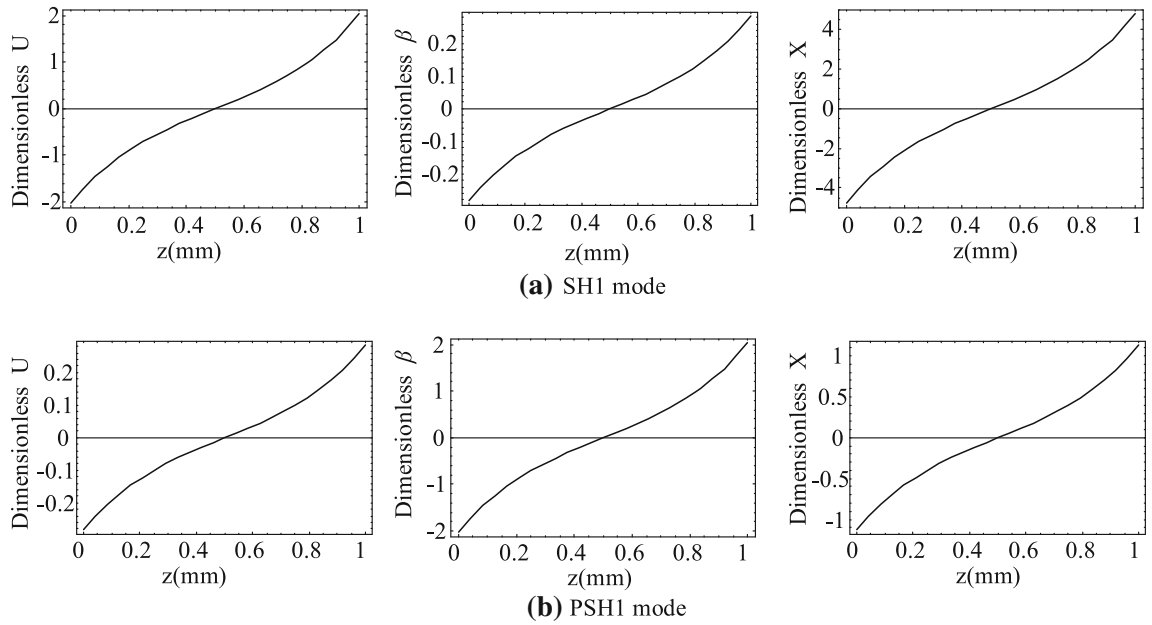

Fig. 14 Displacement and electric potential distributions of SH waves at $kh = 1$

The displacement and electric potential distributions of SH waves at $kh = 1$ are illustrated in Fig. 14. The phason displacements and electric potentials have the same distribution trends with those of the phonon displacement components V in the quasi-periodic direction. The reason lies in the fact that terms in Eq. (18.1) related to the phason displacements and electric potential are similar to those of the phonon displacement component in the y-direction.

3.4.2 The piezoelectric effect on SH waves

In this Subsection, the piezoelectric effects on SH waves are also investigated. Figure 15 shows the phase velocity dispersion curves of SH waves for the piezoelectric and elastic quasi-crystal plates. In comparison with Fig. 6, the piezoelectric effects make the phase velocity of phonon and phason modes increase, which is consistent with that of Lamb waves.

Subsequently, the influence of electric parameters on the piezoelectric effects are investigated. Figure 16 shows the dispersion curves of SH waves with enlarged piezoelectric parameters e_{ij}. For phonon and phason modes, the phase velocity increases as e_{ij} increase. Compared with Fig. 7, the influence of e_{ij} on SH waves is different from that on Lamb waves.

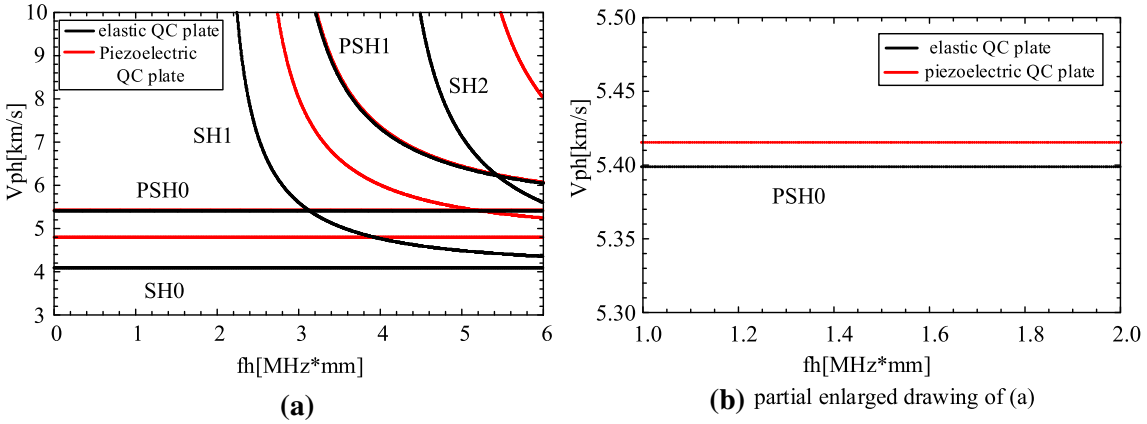

Fig. 15 Phase velocity dispersion curves of SH waves for the piezoelectric quasi-crystal and the elastic quasi-crystal plates

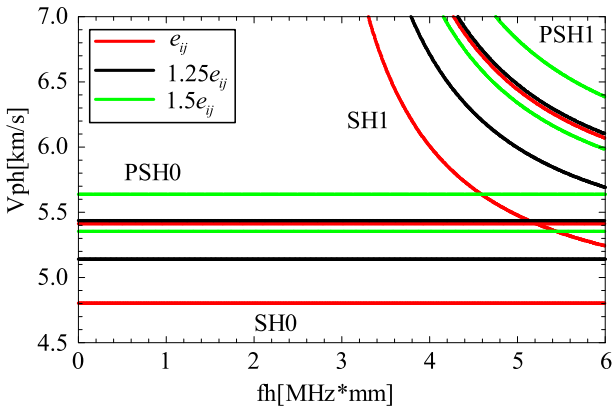

Fig. 16 Phase velocity dispersion curves for the piezoelectric quasi-crystal plate with enlarged piezoelectric parameters e_{ij} in the phonon field

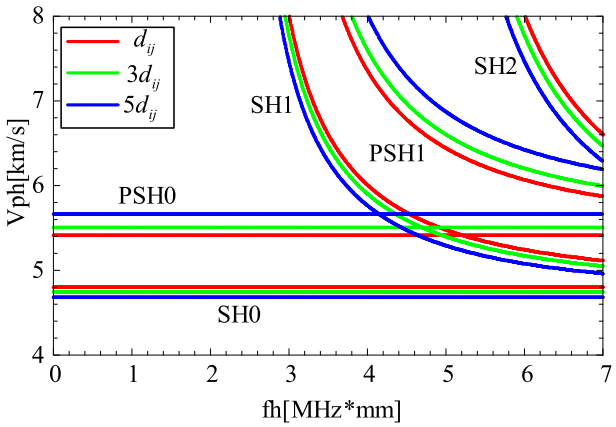

Fig. 17 Phase velocity dispersion curves for the piezoelectric quasi-crystal plate with enlarged piezoelectric parameters d_{ij} in the phason field

Then, the influence of piezoelectric parameters d_{ij} on SH waves is investigated, and the dispersion curves with enlarged piezoelectric parameters d_{ij} are illustrated in Fig. 17. It can be seen that the influence of d_{ij} on phonon and phason modes is opposite, i.e., as d_{ij} increases, the phase velocity of phason modes increases, and that of phonon modes decreases.

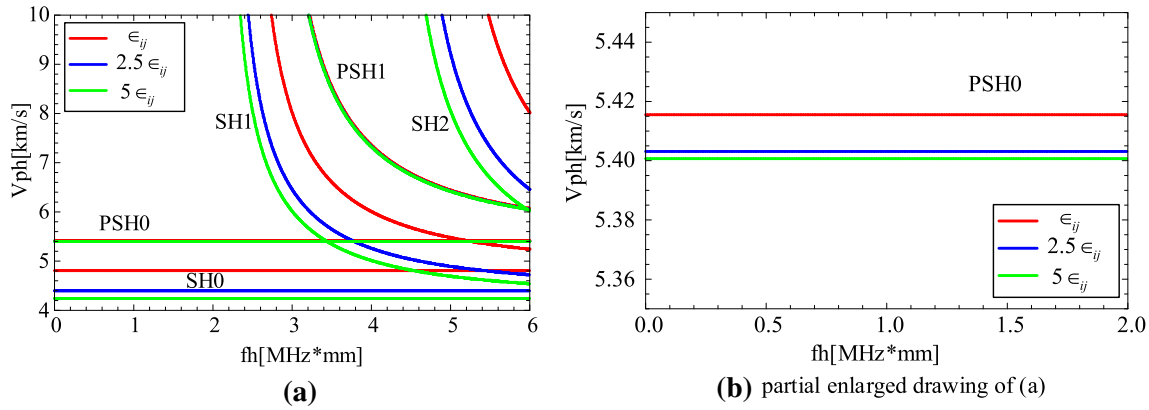

Fig. 18 Phase velocity dispersion curves for the piezoelectric quasi-crystal plate with enlarged dielectric coefficients $\in_{ij}$ in the phason field

At last, Fig. 18 illustrates the phase velocity dispersion curves of SH waves with enlarged dielectric coefficients $\in_{ij}$. Compared with Fig. 9, the influence of the dielectric coefficients $\in_{ij}$ on the dispersion curves of Lamb and SH waves is consistent.

4 Conclusions

In the context of Bak's model, the Legendre polynomial method is utilized to investigate Lamb and SH wave propagation in the 1-D hexagonal piezoelectric quasi-crystal plate. The dispersion curves, displacement, and electric potential distributions in the phonon and phason fields are illustrated. The phonon–phason coupling and piezoelectric effects on the dispersion curves are analyzed. Based on the above numerical results, the following conclusions can be drawn:

(i) For the Lamb waves, the phase velocity of phason modes always decreases as the phonon–phason coupling coefficients R_i increase. However, the phase velocity of phason modes for SH waves always increases as the phonon–phason coupling coefficients R_i increase.
(ii) The piezoelectric effects make the phase velocity of Lamb and SH waves increase. And the influence of varied piezoelectric parameters in the phonon and phason fields on wave characteristics is different. It provides a way to regulate the piezoelectric effect of piezoelectric devices.
(iii) The phason displacement and electric potential of Lamb waves and SH waves have the same distribution trends with those of phonon displacement components in the quasi-periodic direction, which lays the theoretical basis for the design and optimization of piezoelectric devices.
(iv) The amplitudes of phason displacement components for the phonon modes are smaller than those of the phonon displacement components. And it is opposite to the phason modes. This characteristic can be used to distinguish the phonon and phason modes.

Acknowledgements The authors gratefully acknowledge the support by the National Natural Science Foundation of China (No. U1804134 and No. 51975189), the Program for Innovative Research Team of Henan Polytechnic University (No. T2017-3) and the Training Plan of Young Key Teachers of Universities in Henan Province (No. 2018-GGJS-060).

APPENDIX

The coefficients in Eq. (9.1), $M_{m,j}$ and $A_{\alpha\gamma}^{m,j}$ $(\alpha, \gamma = 1, 2, 3)$, are as follows:

$$A_{11}^{m,j} = -C_{11} \times k^2 \times u[m, j, 0, 0] + C_{55} \times u[m, j, 0, 2] + C_{55} \times K[m, j, 0, 1],$$
$$A_{12}^{m,j} = (C_{13} + C_{55}) \times i \times k \times u[m, j, 0, 1] + C_{55} \times i \times k \times K[m, j, 0, 0],$$
$$A_{13}^{m,j} = (R_1 + R_3) \times i \times k \times u[m, j, 0, 1] + R_3 \times i \times k \times K[m, j, 0, 0],$$

$$
\begin{aligned}
A_{14}^{m,j} &= (e_{15}+e_{31})\times i\times k\times u[m,\,j,\,0,\,1]+e_{15}\times i\times k\times K[m,\,j,\,0,\,0],\\
A_{21}^{m,j} &= (C_{13}+C_{55})\times i\times k\times u[m,\,j,\,0,\,1]+C_{13}\times i\times k\times K[m,\,j,\,0,\,0],\\
A_{22}^{m,j} &= -C_{55}\times k^2\times u[m,\,j,\,0,\,0]+C_{33}\times u[m,\,j,\,0,\,2]+C_{33}\times K[m,\,j,\,0,\,1],\\
A_{23}^{m,j} &= -R_3\times k^2\times u[m,\,j,\,0,\,0]+R_2\times u[m,\,j,\,0,\,2]+R_2\times K[m,\,j,\,0,\,1],\\
A_{24}^{m,j} &= -e_{15}\times k^2\times u[m,\,j,\,0,\,0]+e_{33}\times u[m,\,j,\,0,\,2]+e_{33}\times K[m,\,j,\,0,\,1],\\
A_{31}^{m,j} &= (R_1+R_3)\times i\times k\times u[m,\,j,\,0,\,1]+R_1\times i\times k\times K[m,\,j,\,0,\,0],\\
A_{32}^{m,j} &= -R_3\times k^2\times u[m,\,j,\,0,\,0]+R_2\times u[m,\,j,\,0,\,2]+R_2\times K[m,\,j,\,0,\,1],\\
A_{33}^{m,j} &= -\mathrm{K}_2\times k^2\times u[m,\,j,\,0,\,0]+\mathrm{K}_1\times u[m,\,j,\,0,\,2]+\mathrm{K}_1\times K[m,\,j,\,0,\,1],\\
A_{34}^{m,j} &= -d_{15}\times k^2\times u[m,\,j,\,0,\,0]+d_{33}\times u[m,\,j,\,0,\,2]+d_{33}\times K[m,\,j,\,0,\,1],\\
A_{41}^{m,j} &= (e_{15}+e_{31})\times i\times k\times u[m,\,j,\,0,\,1]+e_{31}\times i\times k\times K[m,\,j,\,0,\,0],\\
A_{42}^{m,j} &= -e_{15}\times k^2\times u[m,\,j,\,0,\,0]+e_{33}\times u[m,\,j,\,0,\,2]+e_{15}\times K[m,\,j,\,0,\,1],\\
A_{43}^{m,j} &= -d_{15}\times k^2\times u[m,\,j,\,0,\,0]+d_{33}\times u[m,\,j,\,0,\,2]+d_{33}\times K[m,\,j,\,0,\,1],\\
A_{44}^{m,j} &= \in_{11}\times k^2\times u[m,\,j,\,0,\,0]-\in_{33}\times u[m,\,j,\,0,\,2]-\in_{33}\times K[m,\,j,\,0,\,1],\\
M_{m,j} &= -\rho\times u[m,\,j,\,0,\,0]
\end{aligned}
$$

where $u[m,\,j,\,n,\,p]=\int_a^b \pi(z)\times Q_j(z)\times z^n\times\frac{\partial^p Q_m(r)}{\partial r^p}dz$,

$$K[m,\,j,\,n,\,p]=\int_a^b \frac{\partial\pi(z)}{\partial z}\times Q_j(z)\times z^n\times\frac{\partial^p Q_m(r)}{\partial r^p}dz.$$

References

1. Stephens, P.W., Goldman, A.I.: Metallic phase with long-range orientational order and no translational symmetry. Phys. Rev. Lett. **53**(20), 1951–1953 (1984)
2. Fan, C.Y., Li, Y., Xu, G.T., Zhao, M.H.: Fundamental solutions and analysis of three-dimensional cracks in one-dimensional hexagonal piezoelectric quasicrystals. Mech. Res. Commun. **74**, 39–44 (2016)
3. Lee, K., Hsu, J., Naugle, D., Liang, H.: Multi-phase quasicrystalline alloys for superior wear resistance. Mater. Des. **108**, 440–447 (2016)
4. Olsson, S., Broitman, E., Garbrecht, M., et al.: Mechanical and tribological properties of AlCuFe quasicrystal and Al(Si)CuFe approximant thin films. J. Mater. Res. **31**(2), 232–240 (2016)
5. Miglierini, M., Nasu, S.: Magnetic-electronic and structural properties of icosahedral quasicrystals. Mater. Trans. **34**(2), 178–187 (2007)
6. Kenzari, S., Bonina, D., Dubois, J.M., et al.: Quasicrystal-polymer composites for selective laser sintering technology. Mater. Des. **35**, 691–695 (2012)
7. Altay, G., Dokmeci, M.C.: On the fundamental equations of piezoelasticity of quasicrystal media. Int. J. Solids Struct. **49**(23–24), 3255–3262 (2012)
8. Yu, J., Guo, J.H., Pan, E., et al.: General solutions of plane problem in one-dimensional quasicrystal piezoelectric materials and its application on fracture mechanics. Appl. Math. Mech. **36**(6), 793–814 (2015)
9. Li, Y.D., Bao, R., Chen, W.Q.: Axial shear fracture of a transversely isotropic piezoelectric quasicrystal cylinder: Which field (phonon or phason) has more contribution. Eur. J. Mech. A Solid **71**, 179–186 (2018)
10. Tupholme, G.E.: A non-uniformly loaded anti-plane crack embedded in a half-space of a one-dimensional piezoelectric quasicrystal. Meccanica **53**, 73–983 (2018)
11. Zhang, L., Zhang, Y., Gao, Y.: General solutions of plane elasticity of one-dimensional orthorhombic quasicrystals with piezoelectric effect. Phys. Lett. A **378**(37), 2768–2776 (2014)
12. Zhou, Y.B., Li, X.F.: Two collinear mode-III cracks in one-dimensional hexagonal piezoelectric quasicrystal strip. Eng. Fract. Mech. **189**, 133–147 (2017)
13. Wu, D., Zhang, L., Xu, W., et al.: Electroelastic Green's function of one-dimensional piezoelectric quasicrystals subjected to multi-physics loads. J. Intell. Mater. Syst. Struct. **28**(12), 1651–1661 (2016)
14. Bak, P.: Symmetry, stability, and elastic properties of icosahedral incommensurate crystals. Phys. Rev. B Condens. Matter **32**(9), 5764–5772 (1985)
15. Tupholme, G.E.: One-dimensional piezoelectric quasicrystals with an embedded moving, non-uniformly loaded shear crack. Acta Mech. **228**(2), 547–560 (2017)
16. Waksmanski, N., Pan, E., Yang, L.Z., et al.: Free vibration of a multilayered one-dimensional quasi-crystal plate. J. Vib. Acoust. **136**(4), 041019 (2014)

17. Waksmanski, N., Pan, E., Yang, L.Z., et al.: Harmonic response of multilayered one-dimensional quasicrystal plates subjected to patch loading. J. Sound Vib. **375**, 237–253 (2016)
18. Yang, L., Li, Y., Gao, Y., et al.: Three-dimensional exact electric-elastic analysis of a multilayered two-dimensional decagonal quasicrystal plate subjected to patch loading. Compos. Struct. **171**, 198–216 (2017)
19. Sladek, J., Sladek, V., Pan, E.: Bending analyses of 1D orthorhombic quasicrystal plates. Int. J. Solids Struct. **50**(24), 3975–3983 (2013)
20. Chellappan, V., Gopalakrishnan, S., Mani, V.: Control of wave propagation response using quasi crystals: a formulation based on spectral finite element. Mech. Adv. Mater. Struct. **1**, 1–22 (2018)
21. Li, X.F.: A general solution of elasto-hydrodynamics of two-dimensional quasicrystals. Philos. Mag. Lett. **91**(4), 313–320 (2011)
22. Chiang, Y.C., Young, D.L., Sladek, J., et al.: Local radial basis function collocation method for bending analyses of quasicrystal plates. Appl. Math. Modell. **50**, 463–483 (2017)
23. Wang, X., Pan, E.: Analytical solutions for some defect problems in 1D hexagonal and 2D octagonal quasicrystals. Pramana **70**(5), 911–933 (2008)
24. Lefebvre, J.E., Yu, J.G., Ratolojanahary, F.E., et al.: Mapped orthogonal functions method applied to acoustic waves-based devices. AIP Adv. **6**, 065307 (2016)
25. Amor, M.B., Mohamed, H., Ben, G.: Lamb waves propagation in functionally graded piezoelectric materials by Peano-series method. Ultrasonics **55**, 10–14 (2015)
26. Zhang, X., Xu, X., Wang, Y.: Wave propagation in piezoelectric rods with rectangular cross sections. J. Theor. Appl. Mech. **53**(3), 673–682 (2014)